Concave diffraction gratings fabricated with planar lithography.

S. Grabarnik*, A. Emadi, H. Wu, G. De Graaf and R.F. Wolffenbuttel

Electronic Instrumentation Lab., Fac. EEMCS., Delft University of Technology, Mekelweg 4, 2628 CD, Delft, The Netherlands.

ABSTRACT

This paper reports on the development and validation of a new technology for the fabrication of variable line-spacing non-planar diffraction gratings to be used in compact spectrometers. The technique is based on the standard lithographic process commonly used for pattern transfer onto a flat substrate. The essence of the technology presented here is the lithographic fabrication of a planar grating structure on top of a flexible membrane on a glass or silicon wafer and the subsequent deformation of the membrane using a master shape. For the validation of the proposed technology we fabricated several reflection concave diffraction gratings with the f-numbers varying from 2 to 3.8 and a diameter in the 4 – 7 mm range. A glass wafer with circular holes was laminated by dry-film resist to form the membranes. Subsequently, standard planar lithography was applied to the top part of the membranes for realizing grating structures. Finally the membranes were deformed using plano-convex lenses in such a way that precise lens alignment is not required. A permanent non-planar structure remains after curing. The imaging properties of the fabricated gratings were tested in a three-component spectrograph setup in which the cleaved tip of an optical fiber served as an input slit and a CCD camera was used as a detector. This simple spectrograph demonstrated subnanometer spectral resolution in the 580 – 720 nm range.

Keywords: Concave diffraction gratings, diffraction grating fabrication technology, spectrometers

1. INTRODUCTION

The growing number of applications of compact spectroscopic devices has prompted research in the area of spectrometer design and the development of miniature dispersion elements, detectors and optics. The very attractive approach to the design of a compact spectrometer is to use MEMS technologies for the fabrication of spectrometer components, which makes it possible to achieve a small component size, low production cost per item and provides the possibility to integrate several components on the same wafer, thus reducing assembling and alignment work. Various spectrometers fabricated with MEMS technologies were reported in the literature including Fourier Transform Spectrometers [1] and Fabry-Perot tunable spectral filters [2] as well as diffraction grating based spectrometers implemented according to classical principles [3] or in a planar waveguide [4]. In practice it is difficult to obtain spectral resolution below 1 nm over a wide wavelength range with the compact device. For example due to the problems with fabrication of long-stroke MEMS actuators the resolution of miniature Fourier Transform Spectrometers is limited to about 10 nm. Better results can be achieved with diffraction gratings and, as numerical simulations demonstrated, a resolution of 2 nm is possible [4]. In small devices it is always desired to minimize the amount of different components and that is why in miniature spectrometers varied line-space (VLS) gratings combining dispersion and imaging functions are used since these eliminate the need for the collimating and focusing optics. MEMS processing does not easily allow fabrication of non-planar structures and that is why compact spectrometer designs employ flat gratings which allow for the imaging with relatively small optical aberrations only in a narrow wavelength range. To decrease aberrations of the grating one has to limit the input aperture of the spectrometer or correct aberrations with the second planar grating [5]. On the other hand a concave VLS grating introduces much smaller optical aberrations than the planar one and allows for larger input apertures. A standard technique for the fabrication of such gratings is holography. This technique however requires complicated optical recording setup and it can be difficult to satisfy tolerance requirements for the alignment of the setup components and a blank material where grating structure is to be recorded.

*s.grabarnik@tudelft.nl; phone 31 15 278-6285; fax 31 15 278-5755

Moreover, it is not always possible to realize the desired grating structure using holography. The possibility of the fabrication of the concave gratings by replication of the grating structure on the concave lens surface from the elastomer master ("soft lithography") [6] and by laser direct writing [7] were demonstrated. However those techniques do not allow for high throughput, since each grating is fabricated as a single component and there is no possibility for the integration of the grating with other components, if desired. The alignment of the elastomer master relative to the concave lens surface can also be challenging. We developed a technology which overcomes the mentioned problems and possesses the advantages common to MEMS fabrication process. It is based on the planar lithography and thus is compatible with the MEMS processing allowing for the high throughput. The fabrication of the grating structure and its alignment is possible with the accuracy achievable in the standard lithography machine (mask aligner).

2. THEORETICAL CONSIDERATIONS OF THE CONCAVE GRATING

The combination of the dispersion and imaging properties in a single component eliminates the need for an imaging optics simplifying the assembly of a spectrometer considerably. Although planar imaging gratings are relatively easy to fabricate lithographically, their imaging properties are far from desired. Concave gratings can provide much better performance as can be demonstrated using geometrical grating theory [8], [9]. Figure 1 presents a grating imaging point A in to point B.
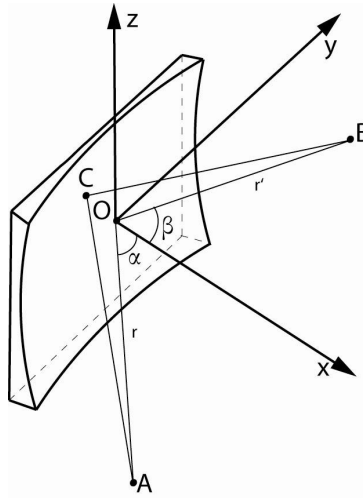

Fig. 1. Imaging geometry of a concave grating.

In the Fig. 1 the center of the coordinate system coincides with the grating central point O, axis ox is directed normally relative to the grating tangent surface and the axes oy and oz are tangent to the grating surface at the point O. Consider point C lying somewhere on the grating surface. Then the path difference between the light traveling from point A to the point B via point O and point C is:

$$F(y,z,\lambda) = ACB - AOB + m\lambda N(y,z) \tag{1}$$

where $N(y, z)$ is a function equal to the number of the grooves between the points O and $C(y, z)$, m is a diffraction order and λ is a wavelength. The function F in Eq. (1) can be decomposed into power series as follows:

$$F(y,z,\lambda) = \sum_{i=0}^{\infty}\sum_{j=0}^{\infty} F_{ij} y^i z^j = \sum_{i=0}^{\infty}\sum_{j=0}^{\infty}\left(M_{ij} + m\lambda N_{ij}\right) y^i z^j , \tag{2}$$

where the coefficients N_{ij} is the result of the decomposition of the function $N(y,z)$:

$$N = \sum_{i=0}^{\infty} \sum_{j=0}^{\infty} N_{ij} y^{i} z^{j} \tag{3}$$

The function $N(y,z)$ can be set equal to an integer number N_g and the shape of the corresponding groove can be found as a dependence $y(z)$ having solved the equation $N_g=N(y,z)$ relative to y. Thus the coefficients N_{ij} are determined by the grating groove pattern. From the definition of the function $N(y,z)$ follows that the local period of the grating can be found as $d = \left(\partial N \big/ \partial y \right)^{-1}$. Using equations for the members of a McLoren series one can obtain:

$$M_{ij} = \frac{1}{i! \, j!} \left[\frac{\partial^{i+j} \left(ACB - AOB \right)}{\partial y^{i} \partial z^{j}} \right]_{(0,0)} \tag{4}$$

The coefficients M_{ij} depend only on the geometry of the grating mounting and the shape of the grating substrate. The grating substrate can be described by a function of $x = f(y,z)$ which can also be decomposed in to McLoren series:

$$x = f(y,z) = \sum_{i=0}^{\infty} \sum_{j=0}^{\infty} a_{ij} y^{i} z^{j} \tag{5}$$

Combining Eqs.(4) and (5) it is possible to obtain analytical formulae for the coefficients M_{ij} (they are listed for example in [9]). Suppose that the system presented in Fig. 1 is symmetrical relative to oy axis. Then the coefficients M_{ij} with j odd are all equal to zero. Other coefficients can be presented as functions of the system parameters:

$$M_{ij} = \varphi(\alpha, \beta, r, r', a_{ij}) \tag{6}$$

The coefficients F_{ij} can be interpreted as the aberration coefficients. Indeed, the path difference F equal to zero corresponds to the spherical wavefront convergent to the point B, and the value of the coefficient F_{ij} determines the deviation of the diffracted wavefront from the spherical one proportional to $y^{i}z^{j}$. For the aberrations free image of a point A at a wavelength λ_0 all the coefficients F_{ij} in Eq. (2) must be made equal to zero. For example, $M_{10} = -(\sin(\alpha) + \sin(\beta))$ and to make $F_{10} = 0$ we have to set $N_{10} = -M_{10} \big/ m\lambda_0$, where λ_0 is the design wavelength. For the wavelengths not equal to λ_0 the coefficient F_{10} can be made zero by choosing another value of the angle β solving the equation $\sin(\alpha) + \sin(\beta) = m\lambda N_{10}$. Thus the value of N_{10} defines the dispersion of the diffraction grating and the period of the grating in its center. For $i>1$ the coefficients F_{ij} must be minimized to reduce aberrations in the desired wavelength range [8]:

$$\int_{\lambda_1}^{\lambda_2} F_{ij}^{2} d\lambda \xrightarrow[M_{ij}, N_{ij}, a_{ij}]{} \min \tag{7}$$

Equations (6) – (7) constitute a system which allows to find the optimal parameters of the grating mounting, the coefficients a_{ij} determining the shape of the grating substrate and N_{ij} responsible for the grating groove pattern. The resolution of a spectrograph is defined by the aberration induced image broadening in the dispersion plane (the xoy plane in Fig. 1). That is why in the following discussion we can consider imaging in this plane assuming $z = 0$. Consider several first members of the series in Eq. (2) which do not include z. The corresponding coefficients are as follows:

$$M_{20} = T(r, \alpha) + T(r', \beta) \tag{8}$$

$$M_{30} = \frac{\sin(\alpha)}{r} T(r, \alpha) + \frac{\sin(\beta)}{r'} T(r', \beta) - a_{30} \big(\cos(\alpha) + \cos(\beta) \big) \tag{9}$$

$$M_{40} = 4\left(\frac{\sin(\alpha)}{r}\right)^2 T(r,\alpha) + 4\left(\frac{\sin(\beta)}{r'}\right)^2 T(r',\beta) -$$

$$-\frac{T(r,\alpha)^2}{r} - \frac{T(r',\beta)^2}{r'} + 4a_{20}\left(\frac{1}{r} + \frac{1}{r'}\right) - \tag{9}$$

$$-8a_{30}\left(\frac{\sin(\alpha)\cos(\alpha)}{r} + \frac{\sin(\beta)\cos(\beta)}{r'}\right) - 8a_{40}\big(\cos(\alpha) + \cos(\beta)\big)$$

$$T(r,\alpha) = \cos(\alpha)\left(\frac{\cos(\alpha)}{2r} - a_{20}\right) \tag{10}$$

Equations (8) – (10) reveal the weakness of a planar grating. For example, the condition for the focusing in the dispersion plane is $F_{20} = 0$ [8]. In case of a planar grating all the coefficients a_{ij} equal to zero, which means that M_{20} is always positive (see Eqs. (8) and (10)). Then, it follows from the Eq. (2) that there is only one wavelength λ_0 at which the focusing ($F_{20} = 0$) can be achieved. As an another example consider a "Rowland" grating [10], which is a grating recorded on a spherical substrate with straight parallel grooves. For this type of gratings $N_{10}=1/d$, where d is the grating constant period and $N_{ij}=0$ for $i>1$, $j>0$. For the spherical substrate $a_{20}=1/2R$, wher R is the radius of substrate curvature. Requiring $F_{20} = 0$ one can obtain the condition for the location of the source and the image points from Eq. (8): $r=R\cos(\alpha)$, $r'=R\cos(\beta)$. These conditions imply that if point A is located on a circle tangent to the point O of a Rowland grating with a radius two times smaller than the radius of curvature of the grating substrate (Rowland circle) the diffraction images will also be located on this circle. Note, that for spectrographs with planar photodetectors the "Rowland" grating is not optimal. The coefficients N_{ij} should be optimized to achieve a plane focal curve. In general, Eq. (6) can be solved by numerical methods, for example using an optical ray tracing software. The best solution usually is a grating with curved not equally separated grooves recorded on an aspherical substrate. The standard technology used for the fabrication of such gratings is holography. After the Eq. (6) is solved, the positions of the recording sources should be reconstructed from the coefficients N_{ij} [8]. However, in some cases it is not possible or a complicated optical setup is required to obtain the desired interfering wavefronts. In this sense a lithography, would it be applicable on the non-planar surfaces, could offer a significant advantage. The coefficients N_{ij} can be used to generate the grating pattern directly on the lithography mask using Eq. (3).

3. FABRICATION TECHNOLOGY

In this article a new technology combining the advantages of a planar lithography with the possibility to produce structures on the non-planar substrates is presented. The key idea of this technique is the fabrication of the grating structure on top of a thin membrane formed on a glass or silicone wafer followed by the deformation of the membrane into the desired shape. Typical values of the F# of diffraction gratings used in spectrometers are in the range of 2 – 4. This implies that the membrane should be stretchable enough to allow for the necessary elongation for the planar membrane to be deformed in a concave spherical surface with such values of the F#. Such elongation can be estimated from the simple geometrical considerations as:

$$\sigma = 2F\#\times\arcsin\left(\frac{1}{2F\#}\right) - 1 \tag{11}$$

Substituting numerical value F#=2 in Eq. (1) one can obtain that the membrane should be capable to survive elongations of about than 1%. Membranes typically used in MEMS (for example SiN) don't allow for such deformation and the only material flexible enough is a polymer. Although several techniques for the polymer membranes fabrication are possible (for example [11]) we tried to find the simplest one. As a result we developed the following process illustrated on the Fig. 1.

The process starting step is the lamination of the glass wafer with through holes at specified locations with the dry film resist as demonstrated on the Fig. 1(a). For the simplicity we consider only one hole in the following discussion. We used OHKA TMMF negative film photoresist [12] which was very easy to work with. However the surface of the resist contains small scratches which can be 1– 20 μm in diameter and 0.1 – 0.5 μm deep. Such defects lead to light scattering

which for the diffraction gratings implies the presence of stray light or noise. In order to decrease the scattering effect of scratches we spincoated a 5 μm thick layer of SU8 resist on top of the TMMF film thus having smoothed its surface (Fig. 1(b)). Then the grating structure with the spatial frequency of 250 line pairs/mm was made lithographically in the second SU8 layer which was 3 μm thick as presented on the Fig.1(c). As a next step the cavity under the membrane was filled with the epoxy adhesive and the wafer was glued to another one. The membrane was deformed with the plano-convex lens as illustrated in Fig. 1(d) and after epoxy is cured the lens was removed.
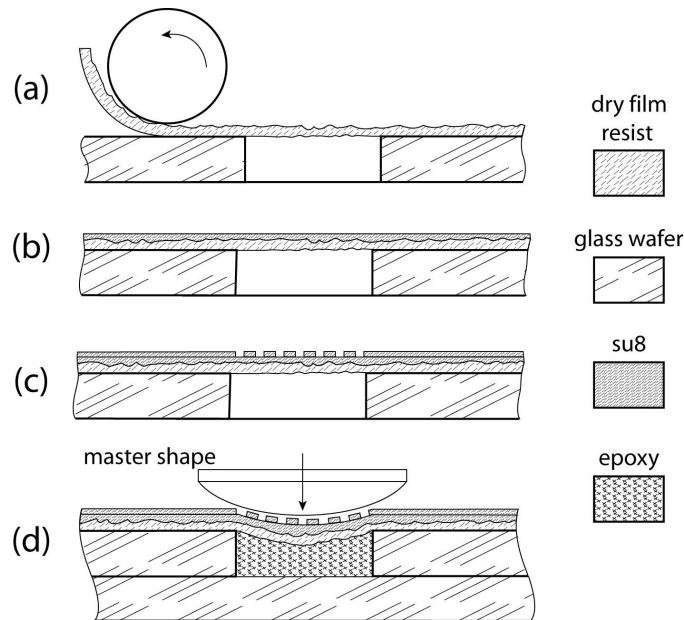
Fig. 2. Concave diffraction grating fabrication process.

Taking into account that the holes diameter was 7 mm and radius of the lens semi-sphere was 25.8 mm the F# number of the produced grating was about 3.6. Finally the grating was covered with a thin layer of aluminum for light reflection. Figure 3 presents a part of the processed wafer containing two concave diffraction gratings. For the fabrication of the grating we used a simple lithography mask consisting of a number of equally spaced lines. Thus the gratings structure was close to that one of a classic Rowland grating with the small differences resulted from the stretching of the membrane. The relative elongation of the membrane after deformation can be estimated from the Eq. (11) to be 0.3%. Thus the imaging properties of the produced gratings should follow the imaging of the Rowland grating.
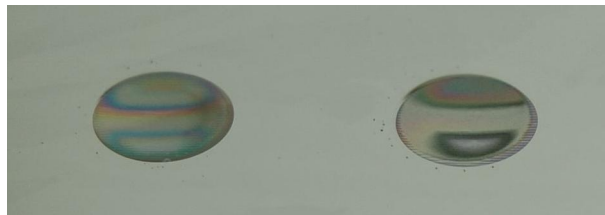

Fig. 3. A part of aluminum coated wafer with two diffraction gratings.

4. EXPERIMENTAL CHARACTERIZATION OF THE GRATINGS.

The roughness of the dry film resist and the surface of the gratings were examined using Scanning Electron Microscope (SEM) and Alfa-step 500 profilomiter. SEM photographs of the dry photoresist surface and the fabricated grating are presented in Fig. 4(a) and Fig. 4(b) respectively. The magnification in Figures 4(a) and 4(b) is the same. The significant defects are clearly visible on the surface of the dry film photoresist in Fig. 4(a). The application of a layer of SU8 has improved the surface quality as it is clear from Fig. 4(b), but some defects still present. The effect of the SU8 layer is visible in Fig 5. Figure 5 presents a dry film resist profile before (Fig. 5(a)) and after (Fig. 5(b)) the spincoating of SU8.
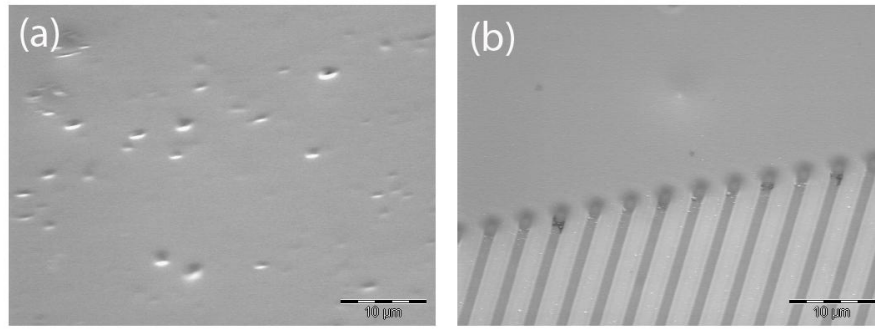
Fig. 4. SEM photograph of the dry resist surface (a) and the edge part of the grating (b).

Due to SU8 the high frequency component of roughness was reduced, but the amplitude of the low frequency component did not change significantly. The coating of the photoresist membrane surface with more layers of SU8 did not decrease significantly the level of the low frequency roughness.
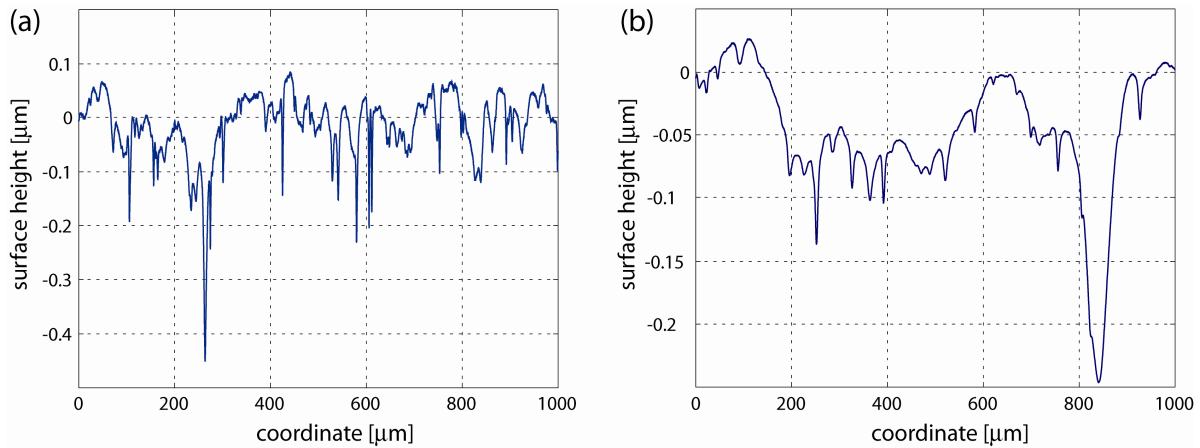

Fig. 5. Scanned profile of the dry film resist (a) and the deviation of the grating profile from circle (b).

Figure 6 presents the processed data of the grating profile scan which was made using profilometer. Original scan data contained a high frequency periodic component which is the result of the periodic grating grooves. This component was removed from the scan profile data using a lowpass filter. Then, the curve fitting optimization procedure was used to approximate the grating profile with a reference circle.
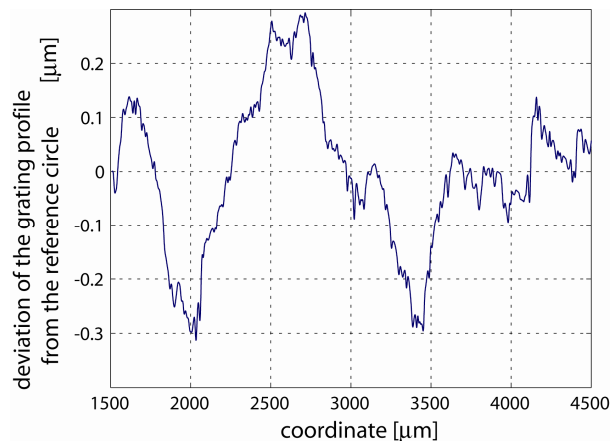

Fig. 6. The deviation of the grating profile from the reference circle.

The difference between the profile of the grating (with the high frequency component filtered out) and the reference circle is shown in Fig. 6. The amplitude of the deviation of the grating profile from the reference is comparable with the roughness in Fig. 5(b). It means that the shape replication errors at least are nor larger than the roughness of the membrane.

The imaging properties of the fabricated gratings were tested in a spectrograph setup shown schematically in Fig. 7.
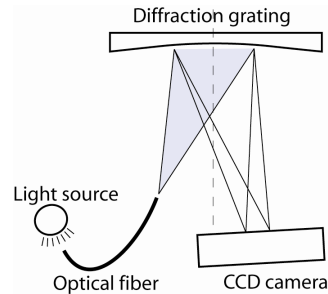

Fig. 7. Spectrograph setup used for the characterization of the gratings.

Light from the Neon lamp was delivered to the grating using optical fiber with 5 microns mode diameter and numerical aperture of 0.11. The cleaved fiber tip served as an input slit of the spectrograph and a CCD camera was used to capture diffracted light. In order to minimize aberrations the fiber tip was located on the "Rowland" circle and the surface of the CCD chip was tangent to this circle. The parameters of the setup were as follows: the distance from the fiber tip to the grating $f1=22$ mm, the distance from the grating to CCD camera $f2=25$ mm and the grating period $d=4$ μm. The spectral pattern registered with the CCD camera and the graphical representation of the obtained spectrum is demonstrated in the Fig. 8. Judging from the width of the spectral lines (FWHM) in the Fig. 8 the resolution of the spectrograph is below 1 nm and the resolving power is $R = \lambda/\Delta\lambda \sim 700$ at wavelength 700 nm. Note that the theoretical limit of the resolving power can be estimated as $R_0=2*NA*f1/d=1210$. The images of the circular fiber tip on the insert in Fig. 8 have elliptical shapes, which are due to the astigmatism of the Rowland grating. It is also visible that the spectral pattern is contaminated with stray light. This effect is explained by scattering resulted from the rough surface of the grating. The ghost lines are also present on the spectrum which is a result of the local deviations of the grating shape from the sphere which are demonstrated in Fig. 6. The local deviations of the surface shape from the spherical one introduce additional aberrations in to the diffracted wavefront and each local defect forms its own image of the entrance slit different from the main image. Such noise images produce ghost or satellite lines accompanying real spectral lines which are marked with thick vertical lines in the Fig 8.
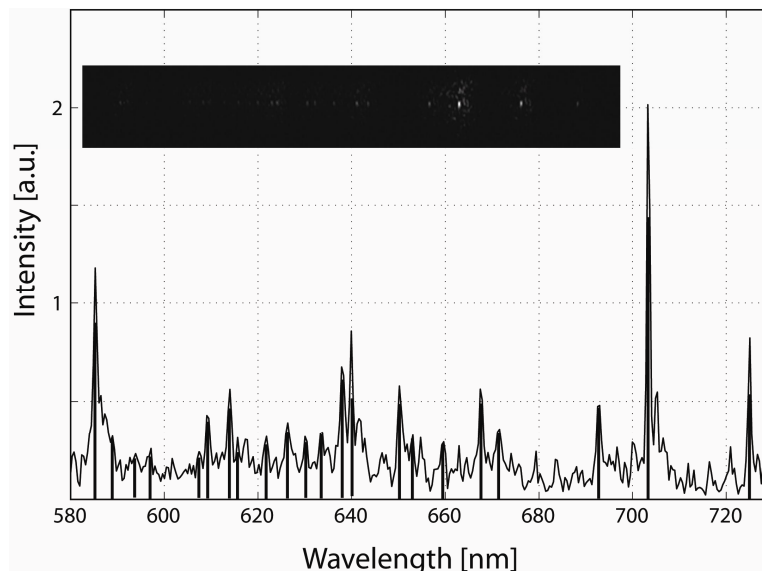

Fig. 8. Ne light spectral pattern captured with the CCD camera and graphical representation of the spectrum.

The presence of satellites makes the measurement of weak spectral lines located close to the strong lines difficult. For example the lines at 724 nm, 703 nm and 693 nm can be easily identified whereas the weak line at 588 nm can not be recognized because of the intensive line at 585 nm.

5. CONCLUSIONS

We have fabricated and characterized concave diffraction gratings using a new technology. This technology is based on a standard lithography and thus is compatible with the MEMS processing and conservers the all the advantages of a planar lithography used for the fabrication of the flat diffraction optical elements. The fabricated gratings were used in a very compact spectrograph setup and allowed for the subnanometer spectral resolution in the visible range. Surface roughness resulted in a stray light and ghost spectral lines which makes the measurements of spectra containing weak spectral lines located close to the strong ones difficult. The scope of our future work is to reduce the level of the stray light and the ghost lines. It can be achieved applying another technology to fabricate the membranes. For example, a layer of su8 can be deposited on one side of the wafer and the through holes can be subsequently etched from the back side with stop on su8. The use of an improved modification of a dry film photoresist can be considered as a second option. The companies producing dry film resist are working to reduce the surface roughness of the film. Thus it can be expected that the level of roughness – induced stray light will be lower with the new resists of higher surface quality.

ACKNOWLEDGMENT

REFERENCES

[1] C. Ataman, H. Urey, and A. Wolter, "A fourier transform spectrometer using resonant vertical comb actuators," J. Micromech. Micro-eng. 16, 2517-2523 (2006)

[2] J. H. Correia, M. Bartek, and R. F.Wolffenbuttel, "Bulk micromachined tunable Fabry–Perot micro-interferometer for the visible spectral range," Sens. Actuators A 76, 191–196 (1999)

[3] S. Ura, F. Okayama, K. Shiroshita, K. Nishio, T. Sasaki, H. Nishihara, T. Yotsuya, M. Okano and K. Satoh, "Planar Reflection Grating Lens for Compact Spectroscopic Imaging System ," Appl. Opt. 42, 175–180 (2003).

[4] I. Avrutsky, K. Chaganti, I. Salakhutdinov and G. Auner, "Concept of a miniature optical spectrometer using integrated optical and micro-optical components," Appl. Opt. 45, 7811–7817 (2006)

[5] S. Grabarnik, R. Wolffenbuttel, A. Emadi, M. Loktev, E. Sokolova, and G. Vdovin, "Planar double-grating microspectrometer," Opt. Express 15, 3581–3588 (2007)

[6] Younan Xia, Enoch Kim, Xiao-Mei Zhao, John A. Rogers, Mara Prentiss, and George M. Whitesides, "Complex Optical Surfaces Formed by Replica Molding Against Elastomeric Masters", Science 273, 347-349 (1996)

[7] D. Radtke and U. D. Zeitner, "Laser-lithography on non-planar surfaces," Opt. Express 15, 1167-1174 (2007)

[8] H. Noda, T. Namioka and M. Seya, "Geometric theory of the grating," J. Opt. Soc. Am. 64, 1031–1036 (1974).

[9] C. Palmer and W.R. McKinney, "Imaging theory of plane-symmetric varied line-space grating systems", Opt. Eng., 33, 820–829 (1994).

[10] H. A. Rowland, "Preliminary notice of the results accomplished in the manufacture and theory of gratings for optical purposes," Phil. Mag. 13, 469 (1882).

[11] C. Friese, M. Wissmann, H. Zappe, H., "Polymer-based membrane mirrors for micro-optical sensors", in Proceedings of IEEE Sensors (IEEE, 2003), pp. 667-672.

[12] http://www.tok.co.jp/en/index.html